# Adaptive Robust Motion Control of Single-Rod Hydraulic Actuators: Theory and Experiments

Bin Yao, *Member, IEEE*, Fanping Bu, John Reedy, and George T.-C. Chiu

***Abstract*—High-performance robust motion control of single-rod hydraulic actuators with constant unknown inertia load is considered. In contrast to the double-rod hydraulic actuators studied previously, the two chambers of a single-rod hydraulic actuator have different areas. As a result, the dynamic equations describing the pressure changes in the two chambers cannot be combined into a single load pressure equation. This complicates the controller design since it not only increases the dimension of the system to be dealt with but also brings in the stability issue of the added internal dynamics. A discontinuous projection-based adaptive robust controller (ARC) is constructed. The controller is able to take into account not only the effect of parameter variations coming from the inertia load and various hydraulic parameters but also the effect of hard-to-model nonlinearities such as uncompensated friction forces and external disturbances. The controller guarantees a prescribed output tracking transient performance and final tracking accuracy in general while achieving asymptotic output tracking in the presence of parametric uncertainties. In addition, the zero error dynamics for tracking any nonzero constant velocity trajectory is shown to be globally uniformly stable. Extensive experimental results are obtained for the swing motion control of a hydraulic arm and verify the high-performance nature of the proposed ARC control strategy. In comparison to a state-of-the-art industrial motion controller, the proposed ARC algorithm achieves more than a magnitude reduction of tracking errors. Furthermore, during the constant velocity portion of the motion, the ARC controller reduces the tracking errors almost down to the measurement resolution level.**

***Index Terms*—Adaptive control, electrohydraulic system, motion control, robust control, servo control.**

## I. Introduction

HYDRAULIC systems have been used in industry in a wide number of applications by virtue of their small size-to-power ratios and the ability to apply very large force and torque; examples like electrohydraulic positioning systems [1], [2], active suspension control [3], and industrial hydraulic machines [4]. However, hydraulic systems also have a number of characteristics which complicate the development of high-performance closed-loop controllers. The dynamics of hydraulic systems are highly nonlinear [5]. Furthermore, the system may be subjected to nonsmooth and discontinuous nonlinearities due to control input saturation, directional change of valve opening, friction, and valve overlap. Aside from the nonlinear nature of hydraulic dynamics, hydraulic systems also have a large extent of model uncertainties. The uncertainties can be classified into two categories: *parametric uncertainties* and *uncertain nonlinearities*. Examples of parametric uncertainties include the large changes in load seen by the system in industrial use and the large variations in the hydraulic parameters (e.g., bulk modulus) due to the change of temperature and component wear [6]. Other general uncertainties, such as the external disturbances, leakage, and friction, cannot be modeled exactly and the nonlinear functions that describe them are not known. These kinds of uncertainties are called uncertain nonlinearities. These model uncertainties may cause the controlled system, designed on the nominal model, to be unstable or have a much degraded performance. Nonlinear robust control techniques, which can deliver high performance in spite of both parametric uncertainties and uncertain nonlinearities, are essential for successful operations of high-performance hydraulic systems.

In the past, much of the work in the control of hydraulic systems has used linear control theory [1], [2], [7]–[9] and feedback linearization techniques [10], [11]. In [3], Alleyne and Hedrick applied the nonlinear adaptive control to the force control of an active suspension driven by a double-rod cylinder, in which only parametric uncertainties of the cylinder are considered. They demonstrated that nonlinear control schemes can achieve a better performance than conventional linear controllers.

In [12], the adaptive robust control (ARC) approach proposed by Yao and Tomizuka in [13]–[15] was generalized to provide a rigorous theoretic framework for the high performance robust control of a double-rod electrohydraulic servo system by taking into account the particular nonlinearities and model uncertainties of the electrohydraulic servo systems. The presented ARC scheme uses smooth projections [13], [16] to solve the design conflicts between adaptive control technique and robust control technique, which is technical and may not be convenient for practical implementation. In [17], the recently proposed discontinuous projection-method-based ARC design [15] is generalized to solve the practical problems associated with smooth projections [12].

This paper continues the work done in [17] and will generalize the results to the electrohydraulic systems driven by single-rod actuators. In contrast to the double-rod hydraulic actuators studied in [17], the areas of the two chambers of a single-rod hydraulic actuator are different. As a result, the two

Manuscript received April 15, 1999; revised January 4, 2000. Recommended by Technical Editor K. Ohnishi. This work was supported in part by the National Science Foundation under CAREER Grant CMS-9734345 and in part by a grant from the Purdue Research Foundation. This paper was presented in part at the 1999 American Control Conference, San Diego, CA, June 2–4.

B. Yao, F. Bu, and G. T.-C. Chiu are with the Ray W. Herrick Laboratory, School of Mechanical Engineering, Purdue University, West Lafayette, IN 47907 USA (e-mail: byao@ecn.purdue.edu; fanping@ecn.purdue.edu; gchiu@ecn.purdue.edu).

J. Reedy is with the Ray W. Herrick Laboratory, School of Mechanical Engineering, Purdue University, West Lafayette, IN 47907 USA (e-mail: reedy@ecn.purdue.edu) and is also with Caterpillar Inc., Peoria, IL 61656 USA.

Publisher Item Identifier S 1083-4435(00)02468-6.

dynamic equations relating the pressure changes in the two chambers to the servovalve opening cannot be combined into a single equation that relates the load pressure to the valve opening as in [3], [5], [12], and [17]. This complicates the controller design since it not only increases the dimension of the system to be dealt with but also brings in the stability issue of the resulting internal dynamics. A discontinuous projection based ARC controller will be constructed to handle various parametric uncertainties and uncertain nonlinearities. Stability of the resulting internal dynamics will be discussed and it will be shown that the zero error dynamics under nonzero constant velocity tracking is globally uniformly stable, which is the *first* theoretical result available in the literature on the stability of zero error dynamics for single-rod hydraulic actuators.

To test the proposed advanced nonlinear ARC strategy, a three-link robot arm (a scaled-down version of the industrial hydraulic machine arm) driven by three single-rod hydraulic cylinders has been set up. Extensive comparative experimental results have been obtained for the swing motion control of the hydraulic arm. Experimental results verify the high-performance nature of the proposed nonlinear ARC approach; in comparison to a state-of-the-art industrial motion controller, the proposed ARC algorithm achieves more than a magnitude reduction of tracking errors. Furthermore, during the constant velocity portion of the motion, the ARC controller reduces the tracking errors almost down to the measurement resolution level.

This paper is organized as follows. Problem formulation and dynamic models are presented in Section II. The proposed nonlinear ARC strategy is given in Section III. Experimental setup and results are presented in Section IV, and conclusions are drawn in Section V.

## II. Problem Formulation and Dynamic Models

The system under consideration is the same as that in [12] and [17], but with a single-rod hydraulic cylinder. The schematic of the system is depicted in Fig. 1. The goal is to have the inertia load to track any specified motion trajectory as closely as possible; an examples would be a machine tool axis [18].

The dynamics of the inertia load can be described by

$$m\ddot{x}_L = P_1A_1 - P_2A_2 - b\dot{x}_L - F_{fc}(\dot{x}_L) + \tilde{f} \tag{1}$$

where

| | |
|---|---|
| $x_L$ | displacement of the load; |
| $m$ | mass of the load; |
| $P_1$ and $P_2$ | pressures inside the two chambers of the cylinder; |
| $A_1$ and $A_2$ | ram areas of the two chambers; |
| $b$ | combined coefficient of the modeled damping and viscous friction forces on the load and the cylinder rod; |
| $F_{fc}$ | modeled Coulomb friction force; |
| $\tilde{f}(t, x_L, \dot{x}_L)$ | lumped uncertain nonlinearities due to external disturbances, the unmodeled friction forces, and other hard-to-model terms. |

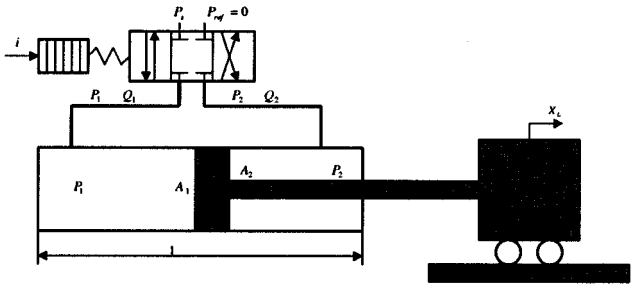

Fig. 1. Single-rod electrohydraulic servo systems.

The actuator (or the cylinder) dynamics can be written as [5]

$$\begin{aligned}\frac{V_1}{\beta_e}\dot{P}_1 &= -A_1\dot{x}_L - C_{tm}(P_1 - P_2) - C_{em1}(P_1 - P_r) + Q_1\\ \frac{V_2}{\beta_e}\dot{P}_2 &= A_2\dot{x}_L + C_{tm}(P_1 - P_2) - C_{em2}(P_2 - P_r) - Q_2\end{aligned} \tag{2}$$

where

| | |
|---|---|
| $V_1 = V_{h_1} + A_1x_L$ | total control volume of the first chamber; |
| $V_2 = V_{h_2} - A_2x_L$ | total control volume of the second chamber; |
| $V_{h1}$ and $V_{h2}$ | two chamber volumes when $x_L = 0$; |
| $\beta_e$ | effective bulk modulus; |
| $C_{tm}$ | coefficient of the internal leakage of the cylinder; |
| $C_{em1}$ | coefficient of the external leakage of the chamber; |
| $C_{em2}$ | coefficient of the external leakage of the chamber; |
| $Q_1$ | supplied flow rate to the forward (or cylinder-end) chamber; |
| $Q_2$ | return flow rate of the return (or rod-end) chamber. |

$Q_1$ and $Q_2$ are related to the spool valve displacement of the servovalve $x_v$ by [5]

$$\begin{aligned}Q_1 &= k_{q1}x_v\sqrt{\Delta P_1}, \quad \Delta P_1 = \begin{cases} P_s - P_1 & \text{for } x_v > 0 \\ P_1 - P_r & x_v < 0 \end{cases}\\ Q_2 &= k_{q2}x_v\sqrt{\Delta P_2}, \quad \Delta P_2 = \begin{cases} P_2 - P_r & \text{for } x_v > 0 \\ P_s - P_2 & x_v < 0 \end{cases}\end{aligned} \tag{3}$$

where

| | |
|---|---|
| $k_{q1}$, $k_{q2}$ | flow gain coefficients of the servovalve; |
| $P_s$ | supply pressure of the fluid; |
| $P_r$ | tank or reference pressure. |

In the experiments, the valve dynamics are neglected and the servovalve opening $x_v$ is directly related to the control input by a known static mapping. However, for the completeness of the theory development, the valve dynamics used by other researchers [19] is included in the following to illustrate how to take into account the effect of valve dynamics if necessary. As in [19], the spool valve displacement $x_v$ is related to the control input $u$ by a first-order system given by

$$\tau_v\dot{x}_v = -x_v + K_vu \tag{4}$$

where $\tau_v$ and $K_v$ are the time constant and gain of the servovalve dynamics, respectively.

As in [17], to minimize the numerical error and facilitate the gain-tuning process, constant scaling factors $S_{c3}$ and $S_{c4}$ are introduced to the pressures and the valve opening, respectively; the scaled pressures are $\overline{P}_1 = (1/S_{c3})P_1$, $\overline{P}_2 = (1/S_{c3})P_2$, $\overline{P}_s = (1/S_{c3})P_s$, $\overline{P}_r = (1/S_{c3})P_r$, and the scaled valve opening is $\overline{x}_v = (1/S_{c4})x_v$. Define the state variables $x = [x_1, x_2, x_3, x_4, x_5]^T \triangleq [x_L, \dot{x}_L, \overline{P}_1, \overline{P}_2, \overline{x}_v]^T$, the entire system, (1)–(4), can be expressed in a state-space form as

$$\begin{aligned}
\dot{x}_1 &= x_2\\
\dot{x}_2 &= \frac{S_{c3}A_1}{m}(x_3 - \overline{A}_c x_4 - \overline{b}x_2 - \overline{F}_{fc}(x_2)) + d(x_1, x_2, t)\\
\dot{x}_3 &= h_1(x_1)\left[\frac{\beta_e S_{c4}k_{q1}}{\sqrt{S_{c3}}V_{h1}}(-\overline{A}_1 x_2 + g_3(x_3, \mathrm{sgn}(x_5))x_5)\right.\\
&\quad \left. - \frac{C_{tm}\beta_e}{V_{h1}}(x_3 - x_4) - \frac{C_{em1}\beta_e}{V_{h1}}(x_3 - \overline{P}_r)\right]\\
\dot{x}_4 &= h_2(x_1)\left[\frac{\beta_e S_{c4}k_{q1}}{\sqrt{S_{c3}}V_{h1}}(\overline{A}_2 x_2 - g_4(x_4, \mathrm{sgn}(x_5))x_5)\right.\\
&\quad \left. + \frac{C_{tm}\beta_e}{V_{h1}}(x_3 - x_4) - \frac{C_{em2}\beta_e}{V_{h1}}(x_4 - \overline{P}_r)\right]\\
\dot{x}_5 &= -\frac{1}{\tau_v}x_5 + \frac{\overline{K}_v}{\tau_v}u
\end{aligned} \tag{5}$$

where $\overline{A}_c = (A_2/A_1)$, $\overline{b} = (b/S_{c3}A_1)$, $\overline{F}_{fc} = (1/S_{c3}A_1)F_{fc}(x_2)$, $d = (1/m)\tilde{f}(t, x_1, x_2)$, $h_1(x_1) = (1/1 + \overline{A}_{h1}x_1)$, $\overline{A}_{h1} = (A_1/V_{h1})$, $\overline{A}_1 = (A_1/k_{q1}S_{c4}\sqrt{S_{c3}})$, $h_2(x_1) = (1/V_{hc} - \overline{A}_{h2}x_1)$, $\overline{A}_{h2} = (A_2/V_{h1})$, $V_{hc} = (V_{h2}/V_{h1})$, $\overline{A}_2 = (A_2/k_{q1}S_{c4}\sqrt{S_{c3}})$, $\overline{K}_v = (K_v/S_{c4})$, and the nonlinear functions $g_3$ and $g_4$ are defined by

$$\begin{aligned}
g_3 &= \sqrt{\overline{\Delta P_1}}, \quad \overline{\Delta P_1} = \begin{cases} \overline{P}_s - x_3 & \text{for } x_5 > 0 \\ x_3 - \overline{P}_r & x_5 < 0 \end{cases}\\
g_4 &= k_{qc}\sqrt{\overline{\Delta P_2}}, \quad \overline{\Delta P_2} = \begin{cases} x_4 - \overline{P}_r & \text{for } x_5 > 0 \\ \overline{P}_s - x_4 & x_5 < 0 \end{cases}
\end{aligned} \tag{6}$$

in which $k_{qc} = (k_{q2}/k_{q1})$ and $\mathrm{sgn}(\bullet)$ is the sign function.

Given the desired motion trajectory $x_{Ld}(t)$, the objective is to synthesize a bounded control input $u$ such that the output $y = x_1$ tracks $x_{Ld}(t)$ as closely as possible in spite of various model uncertainties.

## III. ARC of Single-Rod Hydraulic Acutators

### A. Design Model and Issues to be Addressed

In general, the system is subjected to parametric uncertainties due to the variations of $m$, $b$, $F_{fc}$, $\beta_e$, $C_{tm}$, $C_{em1}$, $C_{em2}$, $\tau$, and $K_v$. For simplicity, in this paper, we only consider the parametric uncertainties due to $m$, $\beta_e$, the leakage coefficients $C_{tm}$, $C_{em1}$, and $C_{em2}$, and $d_n$ (the nominal value of the disturbance $d$). Other parametric uncertainties can be dealt with in the same way if necessary. In order to use parameter adaptation to reduce parametric uncertainties for an improved performance, it is necessary to linearly parametrize the state-space equation (5) in terms of a set of unknown parameters. To achieve this, define the unknown parameter set $\theta = [\theta_1, \theta_2, \theta_3, \theta_4, \theta_5, \theta_6]^T$ as $\theta_1 = (S_{c3}A_1/m)$, $\theta_2 = d_n$, $\theta_3 = (\beta_e S_{c4}k_{q1}/V_{h1}\sqrt{S_{c3}})$, $\theta_4 = (C_{tm}\beta_e/V_{h1})$, $\theta_5 = (C_{em1}\beta_e/V_{h1})$, $\theta_6 = (C_{em2}\beta_e/V_{h1})$. The state-space equation (5) can, thus, be linearly parametrized in terms of $\theta$ as

$$\begin{aligned}
\dot{x}_1 &= x_2\\
\dot{x}_2 &= \theta_1(x_3 - \overline{A}_c x_4 - \overline{b}x_2 - \overline{F}_{fc}(x_2)) + \theta_2 + \tilde{d}(t, x_1, x_2)\\
\dot{x}_3 &= h_1(x_1)[\theta_3(-\overline{A}_1 x_2 + g_3(x_3, \mathrm{sgn}(x_5))x_5)\\
&\quad - \theta_4(x_3 - x_4) - \theta_5(x_3 - \overline{P}_r)]\\
\dot{x}_4 &= h_2(x_1)[\theta_3(\overline{A}_2 x_2 - g_4(x_4, \mathrm{sgn}(x_5))x_5)\\
&\quad + \theta_4(x_3 - x_4) - \theta_6(x_4 - \overline{P}_r)]\\
\dot{x}_5 &= -\frac{1}{\tau_v}x_5 + \frac{\overline{K}_v}{\tau_v}u
\end{aligned} \tag{7}$$

where $\tilde{d} = d - d_n$.

For simplicity, following notations are used throughout the paper: $\bullet_i$ is used for the $i$th component of the vector $\bullet$ and the operation $<$ for two vectors is performed in terms of the corresponding elements of the vectors. The following practical assumption is made.

*Assumption 1:* The extent of parametric uncertainties and uncertain nonlinearities are known, i.e.,

$$\begin{aligned}
\theta &\in \Omega_\theta \triangleq \{\theta\colon \theta_{\min} < \theta < \theta_{\max}\}\\
|\tilde{d}(t, x_1, x_2)| &\le \delta_d(x_1, x_2, t)
\end{aligned} \tag{8}$$

where $\theta_{\min} = [\theta_{1\,\min}, \cdots, \theta_{6\,\min}]^T$, $\theta_{\max} = [\theta_{1\,\max}, \cdots, \theta_{6\,\max}]^T$ and $\delta_d(t, x_1, x_2)$ are known. Physically, $\theta_1 > 0$ and $\theta_3 > 0$. So it is also assumed that $\theta_{1\,\min} > 0$ and $\theta_{3\,\min} > 0$. ◇

At this stage, it is readily seen that the main difficulties in controlling (7) are: 1) the system has unmatched model uncertainties since parametric uncertainties and uncertain nonlinearities appear in equations that do not contain control input $u$; this difficulty can be overcome by employing backstepping ARC design as done in the following; 2) the nonlinear static flow mappings $g_3$ and $g_4$ are functions of $x_5$ also and are *nonsmooth* since they depend on the sign of $x_5$; this prohibits the direct application of the general results in [15] to obtain an ARC controller, which need the differentiability of all terms; and 3) as will become clear later, the "relative degree" [14] of the system is four. Since the system state has a dimension of five, there exists a one-dimensional internal dynamics after an ARC controller is synthesized via backstepping [20]. It is, thus, necessary to check the stability of the resulting internal dynamics, which is a unique feature associated with the control of single-rod hydraulic actuators.

In the following, the discontinuous projection-based ARC design for double-rod hydraulic cylinders [17] will be generalized to overcome the first two difficulties to obtain an ARC controller for (7). To this end, the following notations are introduced.

### B. Notations and Discontinuous Projection Mapping

Let $\hat{\theta}$ denote the estimate of $\theta$ and $\tilde{\theta}$ the estimation error (i.e., $\tilde{\theta} = \hat{\theta} - \theta$). Viewing (8), a simple discontinuous projection can be defined [21], [22] as

$$\mathrm{Proj}_{\hat{\theta}_i}(\bullet_i) = \begin{cases} 0 & \text{if } \hat{\theta}_i = \theta_{i\,\max} \text{ and } \bullet_i > 0 \\ 0 & \text{if } \hat{\theta}_i = \theta_{i\,\min} \text{ and } \bullet_i < 0 \\ \bullet_i & \text{otherwise} \end{cases} \tag{9}$$

where $i = 1, \cdots, 6$. By using an adaptation law given by

$$\dot{\hat{\theta}} = \mathrm{Proj}_{\hat{\theta}}(\Gamma\tau) \tag{10}$$

where $\mathrm{Proj}_{\hat{\theta}}(\bullet) = [\mathrm{Proj}_{\hat{\theta}_1}(\bullet_1), \cdots, \mathrm{Proj}_{\hat{\theta}_6}(\bullet_6)]^T$, $\Gamma > 0$ is a diagonal adaptation rate matrix, and $\tau$ is an adaptation function to be synthesized later. It can be shown [13] that for any adaptation function $\tau$, the projection mapping used in (10) guarantees

$$\begin{aligned} &(\mathbf{P1}) \quad \hat{\theta} \in \overline{\Omega}_\theta \triangleq \{\hat{\theta}\colon \theta_{\min} \le \hat{\theta} \le \theta_{\max}\} \\ &(\mathbf{P2}) \quad \tilde{\theta}^T(\Gamma^{-1}\mathrm{Proj}_{\hat{\theta}}(\Gamma\tau) - \tau) \le 0, \quad \forall\, \tau. \end{aligned} \tag{11}$$

For simplicity, let $\hat{\dot{x}}_2$, $\hat{\dot{x}}_3$, and $\hat{\dot{x}}_4$ represent the calculable part of the $\dot{x}_2$, $\dot{x}_3$, and $\dot{x}_4$, respectively, which are given by

$$\begin{aligned} \hat{\dot{x}}_2 =& \hat{\theta}_1(x_3 - \overline{A}_c x_4 - \overline{b}x_2 - \overline{F}_{fc}(x_2)) + \hat{\theta}_2 \\ \hat{\dot{x}}_3 =& h_1(x_1)[\hat{\theta}_3(-\overline{A}_1 x_2 + g_3 x_5) - \hat{\theta}_4(x_3 - x_4) \\ & - \hat{\theta}_5(x_3 - \overline{P}_r)] \\ \hat{\dot{x}}_4 =& h_2(x_1)[\hat{\theta}_3(\overline{A}_2 x_2 - g_4 x_5) + \hat{\theta}_4(x_3 - x_4) \\ & - \hat{\theta}_5(x_4 - \overline{P}_r)]. \end{aligned} \tag{12}$$

### C. ARC Controller Design

The design parallels the recursive backstepping ARC design in [15] and [17] with an added difficulty as follows.

*Step 1:* Noting that the first equation of (7) does not have any uncertainties, an ARC Lyapunov function can be constructed for the first two equations of (7) directly. Define a switching-function-like quantity as

$$z_2 = \dot{z}_1 + k_1 z_1 = x_2 - x_{2eq}, \quad x_{2eq} \triangleq \dot{x}_{1d} - k_1 z_1 \tag{13}$$

where $z_1 = x_1 - x_{1d}(t)$ is the output tracking error, $x_{1d}(t)$ is the desired trajectory to be tracked by $x_1$, and $k_1$ is any positive feedback gain. Since $G_s(s) = (z_1(s)/z_2(s)) = 1/(s + k_1)$ is a stable transfer function, making $z_1$ small or converging to zero is equivalent to making $z_2$ small or converging to zero. Therefore, the remainder of the design is to make $z_2$ as small as possible with a guaranteed transient performance. Differentiating (13) and noting (7)

$$\begin{aligned} \dot{z}_2 =& \dot{x}_2 - \dot{x}_{2eq}, \quad \dot{x}_{2eq} \triangleq \ddot{x}_{1d} - k_1 \dot{z}_1 \\ =& \theta_1(x_3 - \overline{A}_c x_4 - \overline{b}x_2 - \overline{F}_{fc}(x_2)) + \theta_2 + \tilde{d} - \dot{x}_{2eq}. \end{aligned} \tag{14}$$

Define the load pressure as $P_L = x_3 - \overline{A}_c x_4$. It is, thus, clear from (14) that $P_L$ can be thought as the virtual control input to (14), and the resulting equation has almost the same form as the design equation in Step 1 of the ARC algorithm for double-rod actuators in [17]. Thus, the same ARC design technique can be used to construct an ARC control function $\alpha_2(x_1, x_2, \hat{\theta}_1, \hat{\theta}_2, t)$ for the virtual control input $P_L$ such that the output tracking error $z_1 = x_1 - x_{1d}(t)$ converges to zero or a small value with a guaranteed transient performance. The resulting control function $\alpha_2$ and adaptation function $\tau_2(x_1, x_2, \hat{\theta}_1, \hat{\theta}_2, t)$ are given by

$$\begin{aligned} \alpha_2 =& \alpha_{2a} + \alpha_{2s} \\ \alpha_{2a} =& \overline{b}x_2 + \overline{F}_{fc} + \frac{1}{\hat{\theta}_1}(\dot{x}_{2eq} - \hat{\theta}_2) \\ \alpha_{2s} =& \alpha_{2s1} + \alpha_{2s2} \\ \alpha_{2s1} =& -\frac{1}{\theta_{1,\min}} k_{2s1} z_2, \qquad k_{2s1} \ge ||C_{\phi 2}\Gamma\phi_2||^2 + k_2 \\ \tau_2 =& w_2 \phi_2 z_2, \qquad w_2 > 0 \end{aligned} \tag{15}$$

where $C_{\phi 2}$ a positive-definite (p.d.) constant diagonal matrix to be specified later, $k_2$ is any positive scalar, $w_2$ is a positive weighting factor, and

$$\phi_2 = [\alpha_{2a} - \overline{b}x_2 - \overline{F}_{fc}, 1, 0, 0, 0, 0]^T. \tag{16}$$

In (15), $\alpha_{2a}$ functions as an adaptive control law used to achieve an improved model compensation through online parameter adaptation given by (10), and $\alpha_{2s}$ as a robust control law, in which $\alpha_{2s2}$ is any function satisfying the following conditions:

$$\begin{aligned} &\text{condition 1} \quad z_2[\theta_1\alpha_{2s2} - \tilde{\theta}^T\phi_2 + \tilde{d}] \le \varepsilon_2 \\ &\text{condition 2} \quad z_2\alpha_{2s2} \le 0 \end{aligned} \tag{17}$$

where $\varepsilon_2$ is a positive design parameter which can be arbitrarily small. Essentially, condition 1 of (17) represents the fact that $\alpha_{2s2}$ is synthesized to dominate the model uncertainties coming from both parametric uncertainties $\tilde{\theta}$ and uncertain nonlinearities $\tilde{d}$ with a control accuracy measured by the design parameter $\varepsilon_2$, and condition 2 is to make sure that $\alpha_{2s2}$ is dissipating in nature so that it does not interfere with the functionality of the adaptive control part $\alpha_{2a}$. How to choose $\alpha_{2s2}$ to satisfy constraints like (17) can be found in [14] and [15].

Let $z_3 = P_L - \alpha_2$ denote the input discrepancy. For the positive-semidefinite (p.s.d.) function $V_2$ defined by $V_2 = (1/2)w_2 z_2^2$, using the same technique as in [17], it can be shown that

$$\begin{aligned} \dot{V}_2 =& w_2\theta_1 z_2 z_3 + w_2 z_2(\theta_1\alpha_{2s2} - \tilde{\theta}^T\phi_2 + \tilde{d}) \\ & - w_2 \frac{\theta_1}{\theta_{1\,\min}} k_{2s1} z_2^2. \end{aligned} \tag{18}$$

*Step 2:* In Step 1, as seen from (18), if $z_3 = 0$, output tracking would be achieved by noting (17) and using the standard ARC arguments [15]. Therefore, Step 2 is to synthesize a virtual control function such that $z_3$ converges to zero or a small value with a guaranteed transient performance as follows. From (7) and (15)

$$\begin{aligned} \dot{z}_3 =& \dot{P}_L - \dot{\alpha}_2 \\ =& \theta_3[-(\overline{A}_1 h_1 + \overline{A}_2\overline{A}_c h_2)x_2 + (h_1 g_3 + \overline{A}_c h_2 g_4)x_5] \\ & - \theta_4(x_3 - x_4)(h_1 + \overline{A}_c h_2) - \theta_5 h_1(x_3 - \overline{P}_r) \\ & + \theta_6\overline{A}_c h_2(x_4 - \overline{P}_r) - \dot{\alpha}_{2c} - \dot{\alpha}_{2u} \end{aligned} \tag{19}$$

where

$$\begin{aligned}\dot{\alpha}_{2c} &= \frac{\partial \alpha_2}{\partial x_1} x_2 + \frac{\partial \alpha_2}{\partial x_2} \hat{x}_2 + \frac{\partial \alpha_2}{\partial t} \\ \dot{\alpha}_{2u} &= \frac{\partial \alpha_2}{\partial x_2} [-(x_3 - \overline{A}_c x_4 - \overline{b} x_2 - \overline{F}_{fc})\tilde{\theta}_1 - \tilde{\theta}_2 + \tilde{d}] \\ &\quad + \frac{\partial \alpha_2}{\partial \hat{\theta}} \dot{\hat{\theta}}. \end{aligned} \tag{20}$$

In (20), $\dot{\alpha}_{2c}$ represents the calculable part of $\dot{\alpha}_2$ and can be used in the control function design while $\dot{\alpha}_{2u}$ is the incalculable part due to various uncertainties and has to be dealt with by certain robust feedback as follows.

In (19), the valve opening $x_5$ cannot be treated as the virtual control input for $z_3$ dynamics since both $g_3(x_3, \text{sgn}(x_5))$ and $g_4(x_4, \text{sgn}(x_5))$ contain $\text{sgn}(x_5)$; this important fact has been neglected in most of the previous research due to certain technical requirements. Here, we use a similar strategy as in [12] and [17] to overcome this technical difficulty. Namely, a new virtual control input $Q_L$ is introduced as

$$Q_L = [h_1 g_3(x_3, \text{sgn}(x_5)) + \overline{A}_c h_2 g_4(x_3, \text{sgn}(x_5))] x_5. \tag{21}$$

By doing so, it is readily seen that (19) has essentially the same structure as the design equation in Step 2 of the ARC design [17] for double-rod actuators (although (19) is much more complicated in form). Thus, the same design strategy can be applied to construct a virtual ARC control law $\alpha_3(x_1, x_2, x_3, x_4, \hat{\theta}, t)$ for $Q_L$. The resulting ARC control function $\alpha_3$ and adaptation function $\tau_3(x_1, x_2, x_3, x_4, \hat{\theta}, t)$ are given by

$$\begin{aligned}\alpha_3 &= \alpha_{3a} + \alpha_{3s} \\ \alpha_{3a} &= -\frac{1}{\hat{\theta}_3} \left[ \frac{w_2}{w_3} z_2 \hat{\theta}_1 - \hat{\theta}_3 (\overline{A}_1 h_1 + \overline{A}_2 h_2 \overline{A}_c) x_2 \right. \\ &\quad - \hat{\theta}_4 (h_1 + \overline{A}_c h_2)(x_3 - x_4) - \hat{\theta}_5 h_1 (x_3 - \overline{P}_r) \\ &\quad \left. + \hat{\theta}_6 \overline{A}_c h_2 (x_4 - \overline{P}_r) - \dot{\alpha}_{2c} \right] \\ \alpha_{3s} &= \alpha_{3s1} + \alpha_{3s2}, \\ \alpha_{3s1} &= -\frac{1}{\theta_{3\min}} k_{3s1} z_3 \\ k_{3s1} &\geq k_3 + \left\| \frac{\partial \alpha_2}{\partial \hat{\theta}} C_{\theta 3} \right\|^2 + \| C_{\phi 3} \Gamma \phi_3 \|^2 \\ \tau_3 &= \tau_2 + w_3 \phi_3 z_3 \end{aligned} \tag{22}$$

where $w_3$ is a positive weighting factor, $k_3 > 0$ is a constant, $C_{\theta 3}$ and $C_{\phi 3}$ are p.d. constant diagonal matrices, and

$$\phi_3 = \begin{bmatrix} \dfrac{w_2}{w_3} z_2 - \dfrac{\partial \alpha_2}{\partial x_2} (x_3 - \overline{A}_c x_4 - \overline{b} x_2 - \overline{F}_{fc}) \\ -\dfrac{\partial \alpha_2}{\partial x_2} \\ -(\overline{A}_1 h_1 + \overline{A}_2 \overline{A}_c h_2) x_2 + \alpha_{3a} \\ -(h_1 + \overline{A}_c h_2)(x_3 - x_4) \\ -h_1 (x_3 - \overline{P}_r) \\ \overline{A}_c h_2 (x_4 - \overline{P}_r) \end{bmatrix}. \tag{23}$$

Similar to (17), $\alpha_{3s2}$ is a robust control function satisfying the following two conditions:

$$\begin{aligned} &\text{condition 1} \quad z_3 \left[ \theta_3 \alpha_{3s2} - \tilde{\theta}^T \phi_3 - \frac{\partial \alpha_2}{\partial x_2} \tilde{d} \right] \leq \varepsilon_3 \\ &\text{condition 2} \quad z_3 \alpha_{3s2} \leq 0 \end{aligned} \tag{24}$$

in which $\varepsilon_3$ is a positive design parameter.

Let $z_4 = Q_L - \alpha_3$ be the input discrepancy. Consider the augmented p.s.d. function $V_3$ given by $V_3 = V_2 + (1/2) w_3 z_3^2$. Noting (18), (19), and (22), by straightforward substitutions as in [17], it can be shown that

$$\begin{aligned}\dot{V}_3 &= \dot{V}_2|_{\alpha_2} + w_3 \theta_3 z_3 z_4 + w_3 z_3 \left( \theta_3 \alpha_{3s2} - \tilde{\theta}^T \phi_3 - \frac{\partial \alpha_2}{\partial x_2} \tilde{d} \right) \\ &\quad - w_3 \frac{\theta_3}{\theta_{3\min}} k_{3s1} z_3^2 - w_3 z_3 \frac{\partial \alpha_2}{\partial \hat{\theta}} \dot{\hat{\theta}} \end{aligned} \tag{25}$$

where $\dot{V}_2|_{\alpha_2}$ denotes $\dot{V}_2$ under the condition that $P_L = \alpha_2$ (or $z_3 = 0$).

*Step 3:* Noting the last equation of (7), Step 3 is to synthesize an actual control law for $u$ such that $Q_L$ tracks the virtual control function $\alpha_3$ with a guaranteed transient performance. The problem here is that $Q_L$ is not differentiable at $x_5 = 0$ since it contains $\text{sgn}(x_5)$. Fortunately, noting that $Q_L$ *is differentiable anywhere except at the singular point of* $x_5 = 0$ and is *continuous everywhere*, its left and right derivatives at $x_5 = 0$ exist and are finite. Thus, an actual control input $u$ can still be synthesized to accomplish the job as follows.[1] By the definitions of $Q_L$, $g_3$, and $g_4$, it can be checked out that the derivative of $Q_L$ is given by

$$\begin{aligned}\dot{Q}_L &= \left( \frac{\partial h_1}{\partial x_1} g_3 + \overline{A}_c \frac{\partial h_2}{\partial x_1} g_4 \right) x_5 x_2 + h_1 \frac{\partial g_3}{\partial x_3} \dot{x}_3 x_5 \\ &\quad + \overline{A}_c h_2 \frac{\partial g_4}{\partial x_4} \dot{x}_4 x_5 + (h_1 g_3 + \overline{A}_c h_2 g_4) \dot{x}_5, \quad \forall\, x_5 \neq 0 \end{aligned} \tag{26}$$

where $(\partial h_1/\partial x_1) = -h_1^2 \overline{A}_{h1}$, $(\partial h_2/\partial x_1) = h_2^2 \overline{A}_{h2}$, $(\partial g_3/\partial x_3) = -(\text{sgn}(x_5)/2\sqrt{\Delta P_1})$, and $(\partial g_4/\partial x_4) = (\overline{k}_{qc}\, \text{sgn}(x_5)/2\sqrt{\Delta P_2})$. Noting (7) and (12), $\dot{Q}_L$ can be grouped into three terms as

$$\dot{Q}_L = \dot{Q}_{Lc} + \dot{Q}_{Lu} + (h_1 g_3 + \overline{A}_c h_2 g_4) \frac{\overline{K}_v}{\tau_v} u \tag{27}$$

where

$$\begin{aligned}\dot{Q}_{Lc} &= \left( \frac{\partial h_1}{\partial x_1} g_3 + \overline{A}_c \frac{\partial h_2}{\partial x_1} g_4 \right) x_5 x_2 \\ &\quad + \left( h_1 \frac{\partial g_3}{\partial x_3} \hat{x}_3 + \overline{A}_c h_2 \frac{\partial g_4}{\partial x_4} \hat{x}_4 \right) x_5 \\ &\quad - (h_1 g_3 + \overline{A}_c h_2 g_4) \frac{1}{\tau_v} x_5 \\ \dot{Q}_{Lu} &= h_1 \frac{\partial g_3}{\partial x_3} x_5 h_1 [-\tilde{\theta}_3 (-\overline{A}_1 x_2 + g_3 x_5) \\ &\quad + \tilde{\theta}_4 (x_3 - x_4) + \tilde{\theta}_5 (x_3 - \overline{P}_r)] + \overline{A}_c h_2 \frac{\partial g_4}{\partial x_4} x_5 h_2 \end{aligned}$$

[1]Such an input may experience a finite magnitude jump at $x_5 = 0$, but is allowed in implementation.

$$\cdot[-\tilde{\theta}_3(\overline{A}_2x_2 - g_4x_5) - \tilde{\theta}_4(x_3 - x_4) + \tilde{\theta}_6(x_4 - \overline{P}_r)]. \quad (28)$$

In (27), $\dot{Q}_{Lc}$ and $\dot{Q}_{Lu}$ represent the calculable and incalculable parts of $\dot{Q}_L$, respectively, except the terms involving the control input $u$. Similarly, $\dot{\alpha}_3$ can be grouped into two terms as

$$\dot{\alpha}_3 = \dot{\alpha}_{3c} + \dot{\alpha}_{3u} \quad (29)$$

where

$$\dot{\alpha}_{3c} = \frac{\partial\alpha_3}{\partial x_1}x_2 + \frac{\partial\alpha_3}{\partial x_2}\hat{x}_2 + \frac{\partial\alpha_3}{\partial x_3}\hat{x}_3 + \frac{\partial\alpha_3}{\partial x_4}\hat{x}_4 + \frac{\partial\alpha_3}{\partial t}$$

$$\dot{\alpha}_{3u} = \frac{\partial\alpha_3}{\partial x_2}[-\tilde{\theta}_1(x_3 - \overline{A}_cx_4 - \overline{b}x_2 - \overline{F}_{fc}) - \tilde{\theta}_2 + \tilde{d}] + \frac{\partial\alpha_3}{\partial x_3}h_1[-\tilde{\theta}_3(-\overline{A}_1x_2 + g_3x_5) + \tilde{\theta}_4(x_3 - x_4) + \tilde{\theta}_5(x_3 - \overline{P}_r)] + \frac{\partial\alpha_3}{\partial x_4}h_2[-\tilde{\theta}_3(\overline{A}_2x_2 - g_4x_5) - \tilde{\theta}_4(x_3 - x_4) + \tilde{\theta}_6(x_4 - \overline{P}_r)] + \frac{\partial\alpha_3}{\partial\hat{\theta}}\dot{\hat{\theta}}. \quad (30)$$

Thus, similar to (19), the $z_4$ dynamics can be obtained as

$$\dot{z}_4 = \dot{Q}_L - \dot{\alpha}_3 = \dot{Q}_{Lc} + \dot{Q}_{Lu} + (h_1g_3 + \overline{A}_ch_2g_4)\frac{\overline{K}_v}{\tau_v}u - \dot{\alpha}_{3c} - \dot{\alpha}_{3u}. \quad (31)$$

To design an ARC law for the control input $u$ such that $z_j$, $j = 1, 2, 3, 4$, converge to zero or small values, let us consider the augmented p.s.d. function $V$ given by

$$V = V_3 + \frac{1}{2}w_4z_4^2 = \frac{1}{2}\sum_{j=2}^{4}w_jz_j^2 \quad (32)$$

where $w_4 > 0$. Noting (25) and (31) with (28) and (30), it is straightforward to show that

$$\dot{V} = \dot{V}_3|_{\alpha_3} + w_3\theta_3z_3z_4 + w_4z_4\dot{z}_4 = \dot{V}_3|_{\alpha_3} + w_4z_4\left[\frac{w_3}{w_4}\hat{\theta}_3z_3 + \dot{Q}_{Lc} + (h_1g_3 + \overline{A}_ch_2g_4)\cdot\frac{\overline{K}_v}{\tau_v}u - \dot{\alpha}_{3c} - \tilde{\theta}^T\phi_4 - \frac{\partial\alpha_3}{\partial x_2}\tilde{d} - \frac{\partial\alpha_3}{\partial\hat{\theta}}\dot{\hat{\theta}}\right] \quad (33)$$

where $\dot{V}_3|_{\alpha_3}$ denotes $\dot{V}_3$ under the condition that $Q_L = \alpha_3$ (or $z_4 = 0$), and $\phi_4 = [-(\partial\alpha_3/\partial x_2)(x_3 - \overline{A}_cx_4 + \overline{b}x_2 - \overline{F}_{fc}), -(\partial\alpha_3/\partial x_2), (w_3/w_4)z_3 + (h_1^2(\partial g_3/\partial x_3)x_5 - (\partial\alpha_3/\partial x_3)h_1)(-\overline{A}_1x_2 + g_3x_5) + (\overline{A}_ch_2^2(\partial g_4/\partial x_4)x_5 - (\partial\alpha_3/\partial x_4)h_2)(\overline{A}_2x_2 - g_4x_5), (-h_1^2(\partial g_3/\partial x_3)x_5 + (\partial\alpha_3/\partial x_3)h_1 + \overline{A}_ch_2^2(\partial g_4/\partial x_4)x_5 - (\partial\alpha_3/\partial x_4)h_2)(x_3 - x_4), (-h_1^2(\partial g_3/\partial x_3)x_5 + (\partial\alpha_3/\partial x_3)h_1)(x_3 - \overline{P}_r), (-\overline{A}_ch_2^2(\partial g_4/\partial x_4)x_5 + (\partial\alpha_3/\partial x_4)h_2)(x_4 - \overline{P}_r)]^T$ .

In viewing (33), the following ARC control law $u(x, \hat{\theta}, t)$ and the associated adaptation function $\tau(x, \hat{\theta}, t)$ are proposed:

$$u = u_a + u_s$$

$$u_a = -\frac{\tau_v}{(h_1g_3 + \overline{A}_ch_2g_4)\overline{K}_v}\left[\hat{\theta}_3\frac{w_3}{w_4}z_3 + \dot{Q}_{Lc} - \dot{\alpha}_{3c}\right]$$

$$u_s = u_{s1} + u_{s2},$$

$$u_{s1} = -\frac{\tau_v}{(h_1g_3 + \overline{A}_ch_2g_4)\overline{K}_v}k_{4s1}z_4$$

$$k_{4s1} \geq k_4 + \left\|\frac{\partial\alpha_3}{\partial\hat{\theta}}C_{\theta4}\right\|^2 + \|C_{\phi4}\Gamma\phi_4\|^2$$

$$\tau = \tau_3 + w_4\phi_4z_4 = \sum_{j=2}^{4}w_jz_j\phi_j \quad (34)$$

where $k_4 > 0$, $C_{\theta4}$ and $C_{\phi4}$ are p.d. constant diagonal matrices, and $u_{s2}$ is a robust control function satisfying

$$1) \quad z_4\left[(h_1g_3 + \overline{A}_ch_2g_4)\frac{\overline{K}_v}{\tau_v}u_{s2} - \tilde{\theta}^T\phi_4 - \frac{\partial\alpha_3}{\partial x_2}\tilde{d}\right] \leq \varepsilon_4 \quad (35)$$

$$2) \quad z_4u_{s2} \leq 0$$

in which $\varepsilon_4$ is a design parameter.

### D. Main Results

*Theorem 1:* If controller parameters $C_{\theta j} = \mathrm{diag}\{c_{\theta jl}, l = 1, \cdots, 6\}$, $j = 3, 4$, and $C_{\phi k} = \mathrm{diag}\{c_{\phi kl}\}$, $k = 2, 3, 4$ in (15), (22), and (34) are chosen such that $c_{\phi kl}^2 \geq (3w_k/4)((w_3/c_{\theta3l}^2) + (w_4/c_{\theta4l}^2))$, $\forall k, l$, then, the control law (34) with the adaptation law (10) guarantees the following.

1) In general, the output tracking error $z_1$ and the transformed states $z = [z_1, z_2, z_3, z_4]^T$ are bounded. Furthermore, $V$ given by (32) is bounded above by

$$V(t) \leq \exp(-\lambda_Vt)V(0) + \frac{\varepsilon_V}{\lambda_V}[1 - \exp(-\lambda_Vt)] \quad (36)$$

where $\lambda_V = 2\min\{k_2, k_3, k_4\}$ and $\varepsilon_V = w_2\varepsilon_2 + w_3\varepsilon_3 + w_4\varepsilon_4$.

2) If after a finite time $t_0$, $\tilde{d} = 0$, i.e., in the presence of parametric uncertainties only, then, in addition to results in 1), asymptotic output tracking (or zero final tracking error) is achieved, i.e., $z_1 \longrightarrow 0$ as $t \longrightarrow \infty$. △

*Remark 1:* Results in 1) of Theorem 1 indicate that the proposed controller has an exponentially converging transient performance with the exponentially converging rate $\lambda_V$ and the final tracking error being able to be adjusted via certain controller parameters freely in a *known* form; it is seen from (36) that $\lambda_V$ can be made arbitrarily large, and $(\varepsilon_V/\lambda_V)$, the bound of $V(\infty)$ (an index for the final tracking errors), can be made arbitrarily small by increasing feedback gains $k = [k_2, k_3, k_4]^T$ and/or decreasing controller parameters $\varepsilon = [\varepsilon_2, \varepsilon_3, \varepsilon_3]^T$. Such a guaranteed transient performance is especially important for practical applications since execute time of a run is short. Theoretically, this result is what a well-designed robust controller can achieve. In fact, when the parameter adaptation law (10) is switched off, the proposed ARC law becomes a deterministic robust control law and results 1) of the Theorem remain valid [13], [14].

Result 2) of Theorem 1 implies that the effect of parametric uncertainties can be eliminated through parameter adaptation and an improved performance is obtained. Theoretically, result 2) is what a well-designed adaptive controller can achieve. ◇

*Remark 2:* It is seen from (36) that the transient output tracking error may be affected by the initial value $V(0)$, which may depend on the controller parameters, also. To further

reduce transient tracking error, the reference trajectory initialization can be used as in [14], [15], and [20]. Namely, instead of simply letting the reference trajectory for the controller be the actual desired trajectory or position [i.e., $x_{1d}(t) = x_{Ld}(t)$], the reference trajectory $x_{1d}(t)$ can be generated using a stable fourth-order filter with four initials $x_{1d}(0), \cdots, x_{1d}^{(3)}(0)$ chosen as

$$\begin{aligned} x_{1d}(0) &= x_1(0) \\ \dot{x}_{1d}(0) &= x_2(0) \\ \ddot{x}_{1d}(0) &= \hat{\dot{x}}_2(0) \\ x_{1d}^{(3)}(0) &= \hat{\theta}_1(0)\left[\hat{\dot{x}}_3(0) - \overline{A}_c\hat{\dot{x}}_4(0) - \left(b + \frac{\partial F_{fc}}{\partial x_2}\right)\hat{\dot{x}}_2(0)\right]. \end{aligned} \tag{37}$$

Such a trajectory initialization guarantees that $z_i(0) = 0$, $i = 1, 2, 3, 4$ and $V(0) = 0$. Thus, the transient output tracking error is reduced. It is shown in [14] and [20] that such a trajectory initialization is independent from the choice of controller parameters $k$ and $\varepsilon$ and can be performed offline once the initial state of the system is determined. ♢

*Proof of Theorem 1:* Substituting the control law (34) into (33), it is straightforward to show that

$$\begin{aligned} \dot{V} = &- w_2\frac{\theta_1}{\theta_{1\,\min}}k_{2s1}z_2^2 - w_3\frac{\theta_3}{\theta_{3\,\min}}k_{3s1}z_3^2 - w_4k_{4s1}z_4^2 \\ &+ w_2z_2(\theta_1\alpha_{2s2} - \tilde{\theta}^T\phi_2 + \tilde{d}) \\ &+ w_3z_3\left(\theta_3\alpha_{3s2} - \tilde{\theta}^T\phi_3 - \frac{\partial\alpha_2}{\partial x2}\tilde{d}\right) \\ &+ w_4z_4\left[(h_1g_3 + \overline{A}_ch_2g_4)\frac{\overline{K}_v}{\tau_v}u_{s2} - \tilde{\theta}^T\phi_4 - \frac{\partial\alpha_3}{\partial x_2}\tilde{d}\right] \\ &- \left(w_3z_3\frac{\partial\alpha_2}{\partial\hat{\theta}} + w_4z_4\frac{\partial\alpha_3}{\partial\hat{\theta}}\right)\dot{\hat{\theta}}. \end{aligned} \tag{38}$$

Thus, following the standard discontinuous projection-based ARC arguments as in [15] and [17], the theorem can be proved.[2] □

### *E. Internal Dynamics and Zero Dynamics*

Theorem 1 shows that, under the proposed ARC control law, the *four* transformed system state variables, $z = [z_1, z_2, z_3, z_4]^T \in R^4$, are bounded, from which one can easily prove that the position $x_1$, the velocity $x_2$, and the load pressure $P_L = x_3 - \overline{A}_cx_4$ are bounded. However, since the original system (7) has a dimension of *five*, there exists a one-dimensional internal dynamics, which reflects the physical phenomenon that there exist infinite number sets of pressures in the two chambers of the single-rod actuator to produce the same required load pressure $P_L = x_3 - \overline{A}_cx_4$. In other words, the fact that the load pressure $P_L = x_3 - \overline{A}_cx_4$ and the valve opening $x_5$ are bounded does not necessarily imply that the pressures $x_3$ and $x_4$ in the two chambers of the single-rod cylinder are bounded. It is, thus, necessary to check the stability of the resulting internal dynamics to make sure that the two pressures $x_3$ and $x_4$ are bounded for a bounded control input in implementation. Although simulation and experimental results seem to verify that the two pressures are indeed bounded when tracking a nonzero speed motion trajectory, it is of both practical and theoretical interest to see if we can prove this fact, which is the focus in this section.

Rigorous theoretical proof of the stability of the internal dynamics of a nonlinear system tracking an arbitrary time-varying trajectory is normally very hard and tedious, if not impossible [23]. Bearing this fact in mind, in the following, we take the following pragmatic approach, which is a standard practice in the nonlinear control literature [23]. Namely, instead of looking at the stability of the general internal dynamics directly, we will check the stability of the zero error dynamics for tracking certain typical motion trajectories. For the particular problem studied in this paper, it is easy to verify that the zero error dynamics for tracking a desired trajectory $x_{1d}(t)$ is the same as the internal dynamics when $z(t) = 0$, $\forall\, t$. Thus, if the zero error dynamics is proven to be globally uniformly asymptotically stable, then, it is reasonable to expect that all internal variables are bounded when the proposed ARC law is applied, since $z$ is guaranteed to converge to a small value very quickly by Theorem 1.

Since most industrial operations of hydraulic cylinders involve the tracking of a constant velocity trajectory (e.g., the large portion of the typical point-to-point movement is under constant velocity tracking as shown in the experiments), we will focus on the zero error dynamics associated with the tracking of a nonzero constant velocity trajectory. For these operations, compared with the large control flows needed to maintain the required speed, the leakage flows are typically very small and can be neglected in the analysis for simplicity. The results are summarized in the following theorem.

*Theorem 2:* Assume that the leakage flows can be neglected and the system is absent of uncertain nonlinearities, i.e., $\theta_4 = \theta_5 = \theta_6 = 0$ and $\tilde{d} = 0$ in (7). When tracking any nonzero constant velocity trajectory (i.e., $\dot{x}_{1d}(t) = x_{2d}$ is a nonzero constant), the following results hold.

1) The corresponding pressures of the two chambers and the valve opening have a unique equilibrium; when $x_{2d} > 0$, the unique equilibrium point is given by

$$\begin{aligned} x_{3e} &= \frac{\overline{A}_c^3\overline{P}_s + \overline{A}_ck_{qc}^2\overline{P}_r - k_{qc}^2\left[\dfrac{\theta_2}{\theta_1} - \overline{b}x_{2d} - \overline{F}_{fc}(x_{2d})\right]}{k_{qc}^2 + \overline{A}_c^3} \\ x_{4e} &= \frac{\overline{A}_c^2\overline{P}_s + k_{qc}^2\overline{P}_r + \overline{A}_c^2\left[\dfrac{\theta_2}{\theta_1} - \overline{b}x_{2d} - \overline{F}_{fc}(x_{2d})\right]}{k_{qc}^2 + \overline{A}_c^3} \\ x_{5e} &= \frac{\overline{A}_1}{\sqrt{\overline{P}_s - x_{3e}}}x_{2d} \end{aligned} \tag{39}$$

and when $x_{2d} < 0$,

$$\begin{aligned} x_{3e} &= \frac{\overline{A}_ck_{qc}^2\overline{P}_s + \overline{A}_c^3\overline{P}_r - k_{qc}^2\left[\dfrac{\theta_2}{\theta_1} - \overline{b}x_{2d} - \overline{F}_{fc}(x_{2d})\right]}{{k_{qc}}^2 + \overline{A}_c^3} \\ x_{4e} &= \frac{k_{qc}^2\overline{P}_s + \overline{A}_c^2\overline{P}_r + \overline{A}_c^2\left[\dfrac{\theta_2}{\theta_1} - \overline{b}x_{2d} - \overline{F}_{fc}(x_{2d})\right]}{{k_{qc}}^2 + \overline{A}_c^3} \end{aligned}$$

[2]The details are quite tedious and can be obtained from the authors.

$$x_{5e} = \frac{\overline{A}_1}{\sqrt{x_{3e} - \overline{P}_r}}\, x_{2d} \tag{40}$$

where $x_{3e}$, $x_{4e}$, and $x_{5e}$ are the equilibrium values of the two pressures $x_3$ and $x_4$ and the valve opening $x_5$, respectively.

2) The resulting zero error dynamics is globally[3] uniformly asymptotically stable with respect to the equilibrium values given by (39) or (40). ♢

*Proof of Theorem 2:* When tracking a trajectory with a constant velocity of $x_{2d}$ perfectly, the actual position and velocity would be $x_1(t) = x_{2d}t$ and $x_2(t) = x_{2d}$, respectively. From (7), under the assumption made in Theorem 2, the equilibrium values of the two pressures and the valve opening should satisfy the following equations:

$$\begin{aligned} 0 &= \theta_1(x_{3e} - \overline{A}_c x_{4e} - \overline{b}x_{2d} - \overline{F}_{fc}(x_{2d})) + \theta_2 \\ 0 &= h_1(x_1)\theta_3[-\overline{A}_1 x_{2d} + g_3(x_{3e}, \operatorname{sgn}(x_{5e}))x_{5e}] \\ 0 &= h_2(x_1)\theta_3[\overline{A}_2 x_{2d} - g_4(x_{4e}, \operatorname{sgn}(x_{5e}))x_{5e})]. \end{aligned} \tag{41}$$

When $x_{2d} > 0$, $x_{5e} > 0$, which is physically intuitive (for positive constant velocity, the valve opening has to be positive). Thus, $g_3(x_{3e}, \operatorname{sgn}(x_{5e})) = \sqrt{\overline{P}_s - x_{3e}}$ and $g_4(x_{4e}, \operatorname{sgn}(x_{5e})) = k_{qc}\sqrt{x_{4e} - \overline{P}_r}$. It is, thus, straightforward to verify that (39) is the unique solution to (41). Similarly, when $x_{2d} < 0$, $x_{5e} < 0$ and it can be verified that (40) is the unique solution to (41). This completes the proof of 1) of the theorem.

To prove 2) of the theorem, in the following, we will consider the case when $x_{2d} > 0$ only since the case for $x_{2d} < 0$ can be worked out in the same way. The zero error dynamics—the internal dynamics for tracking such a trajectory perfectly (i.e., $x_1(t) = x_{2d}t$ and $x_2(t) = x_{2d}$)—is described by

$$\begin{aligned} 0 = \dot{x}_2 &= \theta_1(x_3 - \overline{A}_c x_4 - \overline{b}x_{2d} - \overline{F}_{fc}(x_{2d})) + \theta_2 \\ \dot{x}_3 &= h_1(x_1)\theta_3[-\overline{A}_1 x_{2d} + g_3(x_3, \operatorname{sgn}(x_5))x_5] \\ \dot{x}_4 &= h_2(x_1)\theta_3[\overline{A}_2 x_{2d} - g_4(x_4, \operatorname{sgn}(x_5))x_5)]. \end{aligned} \tag{42}$$

From the first equation of (42),

$$x_3 = \overline{A}_c x_4 - \left[\frac{\theta_2}{\theta_1} - \overline{b}x_{2d} - \overline{F}_{fc}(x_{2d})\right] \tag{43}$$

and

$$\dot{x}_3 = \overline{A}_c \dot{x}_4. \tag{44}$$

Substituting the last two equations of (42) into (44), the valve opening $x_5$ of the zero error dynamics is obtained as

$$x_5 = \frac{h_1\overline{A}_1 + h_2\overline{A}_c\overline{A}_2}{h_1 g_3 + h_2\overline{A}_c g_4}\, x_{2d}. \tag{45}$$

Noting that $h_1(x_1)$, $h_2(x_1)$, $g_3(x_3, \operatorname{sgn}(x_5))$ and $g_4(x_4, \operatorname{sgn}(x_5))$ all have to be positive to be physically meaningful,[4] from (45), $x_5 > 0$ for positive $x_{2d}$. Thus,

$$g_3 = \sqrt{\overline{P}_s - x_3} \quad \text{and} \quad g_4 = k_{qc}\sqrt{x_4 - \overline{P}_r}. \tag{46}$$

[3]For all pressures within physical limits.

Let $\tilde{x}_3 = x_3 - x_{3e}$ and $\tilde{x}_4 = x_4 - x_{4e}$ be the pressure perturbations from their equilibrium values. Substituting (45) into the last equation of (42), we have

$$\begin{aligned} \dot{\tilde{x}}_4 = \dot{x}_4 &= h_2\theta_3\, \frac{h_1\overline{A}_2 g_3 - h_1 A_1 g_4}{h_1 g_3 + h_2\overline{A}_c g_4}\, x_{2d} \\ &= h_2\theta_3\, \frac{h_1\overline{A}_1(\overline{A}_c g_3 - g_4)}{h_1 g_3 + h_2\overline{A}_c g_4}\, x_{2d}. \end{aligned} \tag{47}$$

Noting (46), (43), and (39) for $x_{4e}$,

$$\begin{aligned} \overline{A}_c g_3 - g_4 &= \frac{\overline{A}_c^2(\overline{P}_s - x_3) - k_{qc}^2(x_4 - \overline{P}_r)}{\overline{A}_c g_3 + g_4} \\ &= -\frac{(\overline{A}_c^3 + k_{qc}^2)}{\overline{A}_c g_3 + g_4}\, \tilde{x}_4 \end{aligned} \tag{48}$$

Thus, (47) becomes

$$\dot{\tilde{x}}_4 = -\beta(x_3, x_4, t)\tilde{x}_4 \tag{49}$$

where

$$\beta(x_3, x_4, t) = \frac{h_1 h_2 \theta_3 \overline{A}_1(\overline{A}_c^3 + k_{qc}^2)}{(h_1 g_3 + h_2\overline{A}_c g_4)(\overline{A}_c g_3 + g_4)}\, x_{2d}. \tag{50}$$

Noting that $h_1(x_1)$, $h_2(x_1)$, $g_3$, and $g_4$ are all positive functions, $\beta$ defined by (50) is a positive function and is uniformly bounded below by a positive number, i.e., there exists a $c_0 > 0$ such that $\beta \geq c_0$. Thus, from (49), the derivative of the Lyapunov function $V_0(\tilde{x}_4) = (1/2)\tilde{x}_4^2$ is

$$\dot{V}(\tilde{x}_4) = -\beta\tilde{x}_4^2 \leq -c_0\tilde{x}_4^2 \tag{51}$$

which is negative definite with respect to $\tilde{x}_4$. Thus, the origin of the $\tilde{x}_4$ dynamics is globally uniformly asymptotically stable, and $x_4$ is bounded. Similarly, it can be proved that the origin of the $\tilde{x}_3$ dynamics is also globally uniformly stable. This completes the proof of 2) of the theorem. □

*Remark 3:* For the regulation problem (i.e., the desired trajectory $x_{1d}(t)$ is a constant), $x_{2d} = 0$, and it is seen from (41) that the equilibrium pressures are not unique; in fact, any pressures $x_{3e}$ and $x_{4e}$ which satisfy $x_{3e} = \overline{A}_c x_{4e} - [(\theta_2/\theta_1) - \overline{F}_{fc}(0)]$ are a set of equilibrium values. Thus, the zero dynamics for the regulation problem will be at most marginally stable but not asymptotically stable. Further study is needed for the stability of the internal dynamics for the regulation problem, which is one of the focuses of our future research. ♢

## IV. Comparative Experiments

### A. Experiment Setup

To test the proposed nonlinear ARC strategy and study fundamental problems associated with the control of electrohydraulic systems, a three-link robot arm (a scaled-down version of an industrial hydraulic machine arm) driven by three single-rod hydraulic cylinders has been set up at the Ray W. Herrick Laboratory of the School of Mechanical Engineering, Purdue University, West Lafayette, IN. The three hydraulic cylinders

[4]$h_1(x_1)$ and $h_2(x_1)$ represent the effect of the control volumes of the two chambers, which are positive for any operations. $g_3$ and $g_4$ represents the flow gains due to the square roots of pressure drops, which are positive.

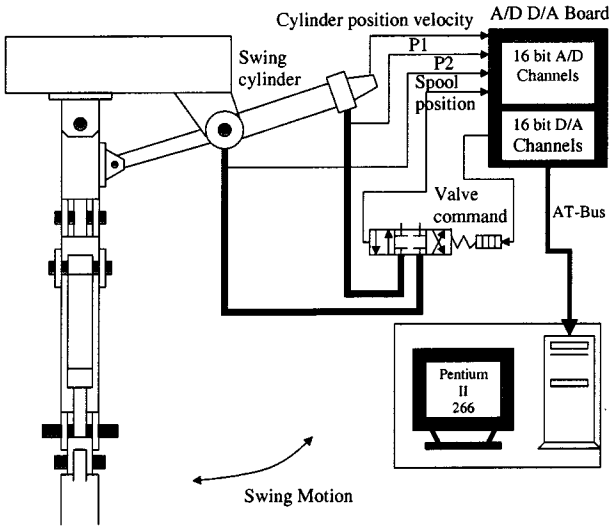


Fig. 2. Experimental setup.

(Parker D2HXTS23A, DB2HXTS23A, and DB2HXT23A) are controlled by two proportional directional control valves (Parker D3FXE01HCNBJ0011) and one servovalve (Parker BD760AAAN10) manufactured by Parker Hannifan Company. Currently, experiments are performed on the swing motion control of the arm (or the first joint) with the other two joints fixed. The schematic of the system is shown in Fig. 2. The swing circuit is driven by a single-rod cylinder (Parker D2HXTS23A with a stroke of 11 in) and controlled by the servovalve. The cylinder has a built-in LVDT sensor, which provides the position and velocity information of the cylinder movement. Pressure sensors (Entran's EPXH-X01-2.5KP) are installed on each chamber of the cylinder. Due to the contaminative noises in the analog signals, the effective measurement resolution for the cylinder position is around 1 mm and the resolution for the pressure is around 15 lbf/in$^2$. Since the range of the velocity provided by the LVDT sensor is too small (less than 0.09 m/s), backward difference plus filter is used to obtain the needed velocity information at high-speed movement. All analog measurement signals (the cylinder position, velocity, forward and return chamber pressures, and the supplied pressure) are fed back to a Pentium II PC through a plugged-in 16-bit A/D and D/A board. The supplied pressure is 1000 lbf/in$^2$.

### *B. System Identification*

For the swing motion shown in Fig. 2, due to the nonlinear transformation between the joint swing angle $q$ and the cylinder position $x_L$, the equivalent mass $m$ of a constant swing inertia seeing at the swing cylinder coordinate depends on the swing angle or the cylinder position $x_L$ as well. However, by restricting the movement of the swing cylinder in its middle range, this equivalent mass $m$ will not change much and, thus, can be treated as constant as assumed in the paper; the equivalent mass is around 2200 kg for the no-load situation. Although tests have been done to obtain the actual friction curve shown in Fig. 3, for simplicity, friction compensation is not used in the following experiments [i.e., let $b = F_{fc} = 0$ in (1)] to test the robustness of the proposed algorithm to these *hard-to-model*

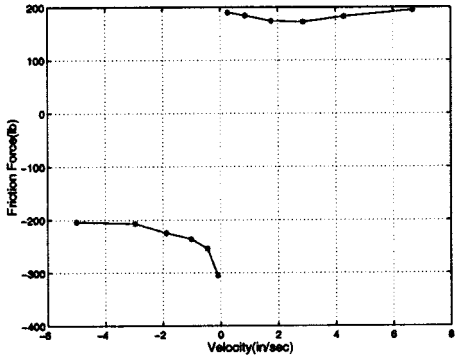


Fig. 3. Friction force.

terms. The cylinder physical parameters are $A_1 = 3.1416$ in$^2$, $A_2 = 1.6567$ in$^2$, $V_{h1} = 30.48$ in$^3$, and $V_{h2} = 55.33$ in$^3$. By assuming no leakage flows and moving the cylinder at different constant velocities, we can back out the static flow mapping of the servovalve (3). The estimated flow gains are $k_{q1} = 0.1820$ in$^3/(\sqrt{\text{psi}}\,\text{s}\,V)$ and $k_{q2} = 0.1886$ in$^3/(\sqrt{\text{psi}}\,\text{s}\,V)$, where the unit for the servovalve opening is normalized in terms of the control voltage supplied to the servovalve at the steady state. Dynamic tests are also performed and reveal that the servovalve dynamics is of second order with a bandwidth around 10 Hz. The effective bulk modulus is estimated around $2.71 \times 10^8$ Pa.

### *C. Controller Simplifications*

Some simplifications suitable for our experiments have been made in implementing the proposed ARC control strategy. First, unlike other experiments [3], [19] where high bandwidth servovalves with spool position feedback is used, our system is designed to mimic typical industrial use of electrohydraulic systems. As such, our system is not equipped with costly sensors to measure the spool displacement of the servovalve for feedback. Furthermore, since a standard industrial servovalve is used, the valve dynamics is actually of a second order with a not-so-high bandwidth around 10 Hz (as opposed to the first-order dynamics (4) used by other researchers [19]). This greatly increases the difficulties in implementing advanced control algorithms if valve dynamics were to be considered in the controller design. To deal with this practical issue, the following pragmatic approach is taken: the valve dynamics are neglected in the controller design stage (i.e., letting $\tau_v = 0$ in the previous ARC controller design) and the closed-loop stability will be achieved by placing the closed-loop bandwidth of the ARC controller below the valve bandwidth with a certain amount of margin as done in the following experiments. With this simplification strategy, the valve opening $x_5$ is related to the control input $u$ by a static gain given by $x_5 = \overline{K}_v u$. Thus, the ARC control design in Step 3 in Section III-C is not needed and the actual control input $u$ is directly calculated based on the control function $\alpha_3$ given by (22) and the static flow mapping (21) with $Q_L$ replaced by $\alpha_3$. The corresponding adaptation function $\tau$ is given by $\tau_3$ in (22). By doing so, the resulting ARC controller is quite simple and yet sufficient, as shown in the comparative experimental results.

The second simplification is made to the selection of the specific robust control term $\alpha_{2s}$ in (15) and $\alpha_{3s}$ in (22). Let $k_{2s}$ and $k_{3s}$ be any nonlinear feedback gains satisfying

$$k_{2s} \geq \frac{1}{\theta_{1\,\min}} \left[ \|C_{\phi 2}\Gamma\phi_2\|^2 + k_2 + \frac{1}{2\varepsilon_2} \left( \|\theta_M\|^2 \|\phi_2\|^2 + \delta_d^2 \right) \right]$$

$$k_{3s} \geq \frac{1}{\theta_{3\,\min}} \left[ k_3 + \left\| \frac{\partial \alpha_2}{\partial \hat{\theta}} C_{\theta 3} \right\|^2 + \|C_{\phi 3}\Gamma\phi_3\|^2 + \frac{1}{2\varepsilon_3} \left( \|\theta_M\|^2 \|\phi_3\|^2 + \left\| \frac{\partial \alpha_2}{\partial x_2} \right\| \delta_d^2 \right) \right] \quad (52)$$

in which $\theta_M = \theta_{\max} - \theta_{\min}$ and $\delta_d$ is defined in (8). Then, using similar arguments as in [15] and [17], one can show that the robust control function of $\alpha_{2s} = -k_{2s}z_2$ satisfies (15) and (17), and $\alpha_{3s} = -k_{3s}z_3$ satisfies (22) and (24).

Knowing the above theoretical results, we may implement the needed robust control terms in the following two ways. The first method is to pick up a set of values for $k_2$, $k_3$, $C_{\phi 2}$, $C_{\phi 3}$, $C_{\theta 3}$, $\varepsilon_2$, and $\varepsilon_3$ to calculate the right-hand side of (52). $k_{2s}$ and $k_{3s}$ can then be determined so that (52) is satisfied for a guaranteed global stability and a guaranteed control accuracy. This approach is rigorous and should be the formal approach to choose. However, it increases the complexity of the resulting control law considerably since it may need significant amount of computation time to calculate the lower bound. As an alternative, a pragmatic approach is to simply choose $k_{2s}$ and $k_{3s}$ large enough without worrying about the specific values of $k_2$, $k_3$, $C_{\phi 2}$, $C_{\phi 3}$, $C_{\theta 3}$, $\varepsilon_2$, and $\varepsilon_3$. By doing so, (52) will be satisfied for certain sets of values of $k_2$, $k_3$, $C_{\phi 2}$, $C_{\phi 3}$, $C_{\theta 3}$, $\varepsilon_2$, and $\varepsilon_3$, at least locally around the desired trajectory to be tracked. In this paper, the second approach is used since it not only reduces the online computation time significantly, but also facilitates the gain tuning process in implementation.

### D. Comparative Experimental Results

Three controllers are tested for comparison:

*1) ARC:* This is the controller proposed in this paper and described in previous sections with the simplification outlined in Section IV-C. For simplicity, in the experiments, only two parameters, $\theta_1$, and $\theta_2$, are adapted; the first parameter represents the effect of the equivalent mass and the second parameter represents the effect of the nominal value of the lumped disturbance. The effect of leakage flows is neglected to test the performance robustness of the proposed algorithm to these terms. Since the valve dynamics is neglected and their bandwidth is not so high (around 10 Hz), not so large feedback gains are used to avoid instability; the control gains used are $k_1 = k_{2s} = k_{3s} = 19$. The scaling factors are $S_{c3} = 2.8085 \times 10^6$ and $S_{c4} = 0.085\,88$ respectively. Weighting factors are $w_2 = w_3 = 1$. Adaptation rates are set at $\Gamma = \mathrm{diag}\{0.01, 0.08\}$.

*2) Deterministic Robust Control (DRC):* This is the same control law as ARC but without using parameter adaptation, i.e., letting $\Gamma = \mathrm{diag}\{0, 0\}$. In such a case, the proposed ARC control law becomes a deterministic robust control law [15].

*3) Motion Controller:* This is the state-of-the-art industrial motion controller (Parker's PMC6270ANI two-axis motion controller) that was bought from Parker Hannifin Company along with the Parker's cylinder and valves used for the experiments. The controller is essentially a proportional plus integral plus derivative (PID) controller with velocity and acceleration feedforward compensation. Controller gains are obtained by strictly following the gain tuning process stated in the *Servo Tuner User Guide* coming with the motion controller [24]. The tuned gains are $SGP = 20$, $SGI = 0.5$, $SGV = 22$, $SGVF = 100$, $SGAF = 0.02$, which represent the P-gain, I-gain, D-gain, the gain for velocity feedforward compensation, and the gain for acceleration feedforward compensation, respectively.

The three controllers are first tested for a slow point-to-point motion trajectory shown in Fig. 4, which has a maximum velocity of $v_{\max} = 0.1$ m/s and a maximum acceleration of $a_{\max} = 0.2$ m/s$^2$. The tracking errors are shown in Fig. 5. As seen, the proposed DRC and ARC have a better performance than the motion controller in terms of both transient and final tracking errors. Due to the use of parameter adaptation as shown in Fig. 8, the final tracking error of ARC is reduced almost down to the position measurement noise level of 1 mm while DRC still has a slight offset. This illustrates the effectiveness of using parameter adaptation, although the estimates do not converge to their true values due to other modeling errors, such as the neglected friction force. The pressures of ARC are shown in Fig. 6, which are regular and, as predicted, are bounded. The control input of ARC is shown in Fig. 7, which is regular.

To test the performance robustness of the proposed algorithms to parameter variations, a 45-kg load is added at the end of the robot arm, which increases the equivalent mass of the cylinder to 4000 kg. The tracking errors are shown in Fig. 9. As seen, even for such a short one-run experiment, the adaptation algorithm of the ARC controller is able to pick up the change of the inertial load (the parameter estimate $\hat{\theta}_1$ shown in Fig. 10 drops quicker than the one in Fig. 8) and an improved performance is achieved in comparison to the nonadaptive DRC. Again, both ARC and DRC exhibit better performance than the motion controller.

The three controllers are then run for a fast point–point motion trajectory shown in Fig. 4, which has a maximum velocity of $v_{\max} = 0.3$ m/s and an acceleration of $a_{\max} = 3$ m/s$^2$; both are near their physical limits. The tracking errors are shown in Fig. 11. As seen, the motion controller cannot handle such an aggressive movement well and a large tracking error around 15–20 mm is exhibited during the constant high-speed movement. In contrast, the tracking error of the proposed ARC during the entire run is kept within 5 mm. Furthermore, the tracking error goes back to the measurement noise level of 1 mm very quickly after the short large acceleration and deceleration periods. As seen from the transient pressures of ARC shown in Fig. 12 and the control input shown in Fig. 13, the system is actually at its full capacity during the short large acceleration and deceleration periods. During the acceleration period, the control input exceeds the maximal output voltage of 10 V while the pressure $P_1$ reaches close to the supplied pressure of 6.897 MPa, and during the deceleration period, $P_1$ is down to reference pressure

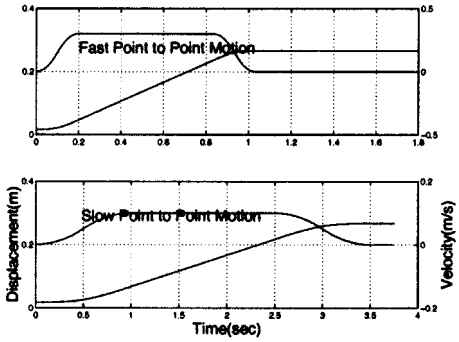


Fig. 4. Point-to-point motion trajectories.

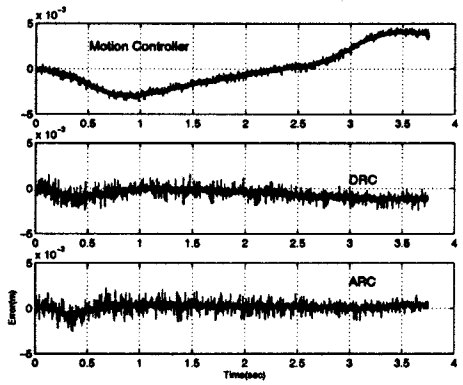


Fig. 5. Tracking errors for slow point-to-point motion without load.

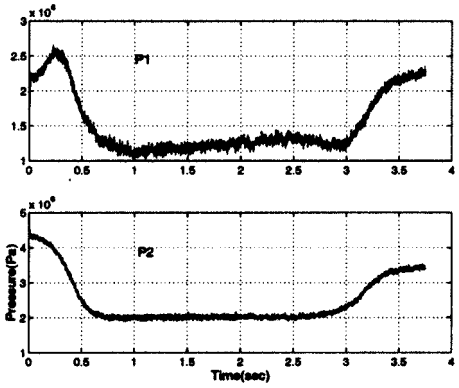


Fig. 6. Pressures for slow point-to-point motion without load.

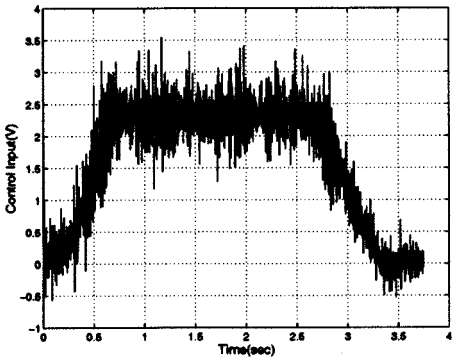


Fig. 7. Control input for slow point-to-point motion without load.

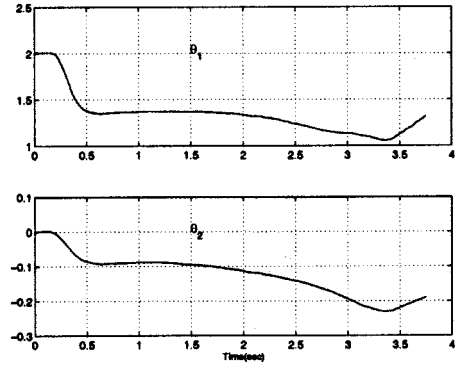


Fig. 8. Parameter estimation for slow point-to-point motion without load.

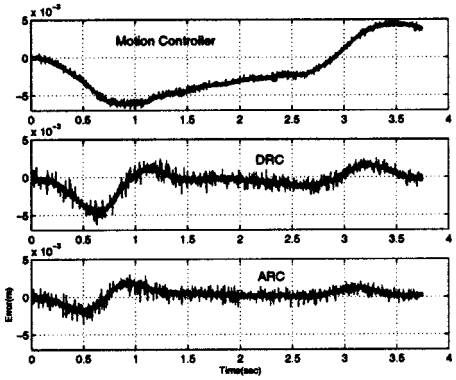


Fig. 9. Tracking errors for slow point-to-point motion with load.

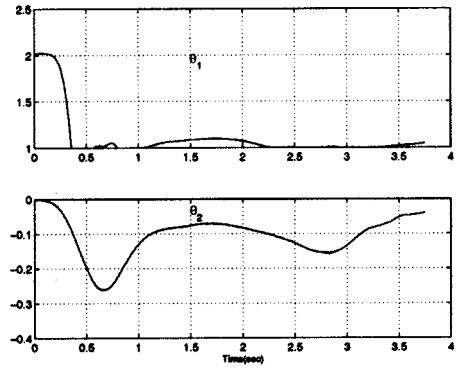


Fig. 10. Parameter estimation for slow point-to-point motion with load.

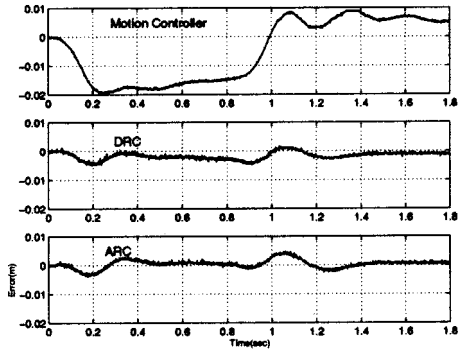


Fig. 11. Tracking errors for fast point-to-point motion without load.

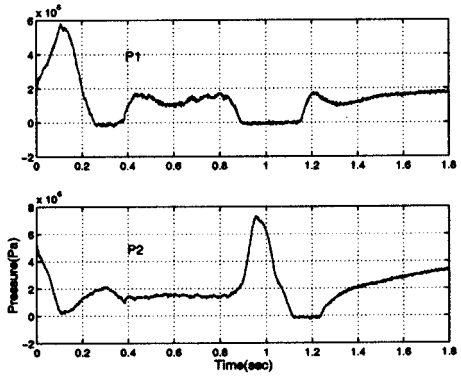


Fig. 12. Pressures for fast point-to-point motion without load.

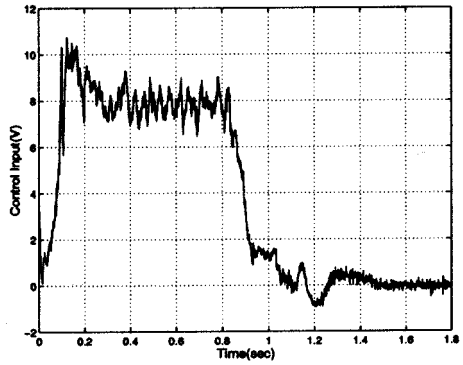


Fig. 13. Control input for fast point-to-point motion without load.

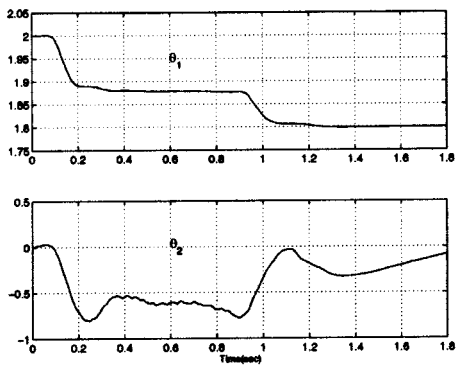


Fig. 14. Parameter estimation for fast point-to-point motion without load.

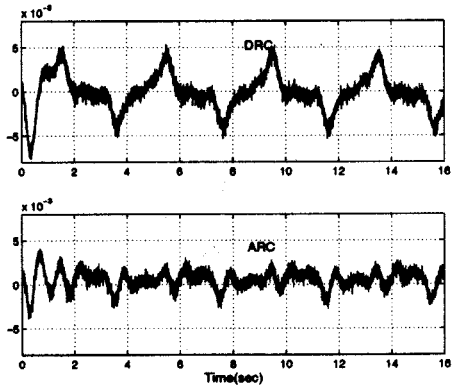


Fig. 15. Tracking errors for fast sine-wave motion with load.

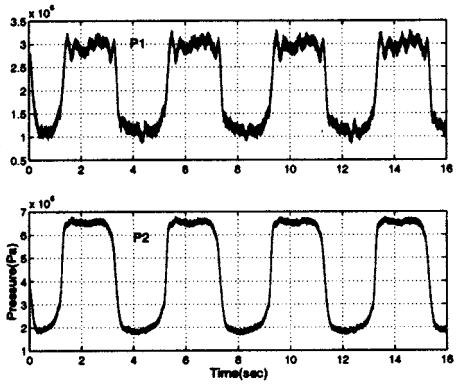


Fig. 16. Pressures for fast sine-wave motion without load.

while $P_2$ reaches the supplied pressure of 6.897 MPa. Despite these difficulties, ARC performs very well as seen in Fig. 11. The parameter estimates are shown in Fig. 14.

Comparative experiments between ARC and DRC are also run for tracking sinusoidal motion trajectories with different frequencies. For example, the tracking errors for tracking a 1/4-Hz sinusoidal trajectory of $0.08\ \sin((\pi/2)t)m$ with load are shown in Fig. 15. As seen, ARC performs better than DRC, which illustrates the effectiveness of using parameter adaptation. The tracking error of ARC is very small, mostly around the measurement resolution of 1 mm, which verifies the high-performance nature of the proposed ARC control strategy. The pressures of ARC are shown in Fig. 16, which are bounded but experience an abrupt change around $t = 1, 3, 5, 7, 9, \cdots$, when the desired velocity changes the direction at those instances. This result qualitatively agrees with the result predicted in 1) of Theorem 2, where the equilibrium values for pressures for positive desired velocity tracking are much different from the equilibrium values for negative desired velocity tracking.

## V. Conclusions

In this paper, a discontinuous projection-based ARC controller has been developed for high-performance robust control of electrohydraulic systems driven by single-rod actuators. The proposed ARC controller takes into account the particular nonlinearities associated with the dynamics of single-rod hydraulic actuators and uses parameter adaptation to eliminate the effect of unavoidable parametric uncertainties due to variations of inertia load and various hydraulic parameters. Uncertain nonlinearities such as external disturbances and uncompensated friction forces are effectively handled via certain robust feedback for a guaranteed robust performance. The controller achieves a guaranteed transient performance and final tracking accuracy for the output tracking while achieving asymptotic output tracking in the presence of parametric uncertainties only. Furthermore, it is shown that the zero error dynamics for tracking any nonzero constant velocity trajectory is globally uniformly stable. Extensive comparative experimental results are obtained for the swing motion of a hydraulic arm. Experimental results verify the high-performance nature of the proposed ARC strategy.

## REFERENCES


[1] P. M. FitzSimons and J. J. Palazzolo, "Part I: Modeling of a one-degree-of-freedom active hydraulic mount," *ASME J. Dynam. Syst., Meas., Contr.*, vol. 118, no. 3, pp. 439–442, 1996.

[2] P. M. FitzSimons and J. J. Palazzolo, "Part II: Control," *ASME J. Dynam. Syst., Meas., Contr.*, vol. 118, no. 3, pp. 443–448, 1996.

[3] A. Alleyne and J. K. Hedrick, "Nonlinear adaptive control of active suspension," *IEEE Trans. Contr. Syst. Technol.*, vol. 3, pp. 94–101, Jan. 1995.

[4] B. Yao, J. Zhang, D. Koehler, and J. Litherland, "High performance swing velocity tracking control of hydraulic excavators," in *Proc. American Control Conf.*, 1998, pp. 818–822.

[5] H. E. Merritt, *Hydraulic Control Systems*. New York: Wiley, 1967.

[6] J. Whatton, *Fluid Power Systems*. Englewood Cliffs, NJ: Prentice-Hall, 1989.

[7] T. C. Tsao and M. Tomizuka, "Robust adaptive and repetitive digital control and application to hydraulic servo for noncircular machining," *ASME J. Dynam. Syst., Meas., Contr.*, vol. 116, no. 1, pp. 24–32, 1994.

[8] A. R. Plummer and N. D. Vaughan, "Robust adaptive control for hydraulic servosystems," *ASME J. Dynam. Syst., Meas., Contr.*, vol. 118, no. 2, pp. 237–244, 1996.

[9] J. E. Bobrow and K. Lum, "Adaptive, high bandwidth control of a hydraulic actuator," *ASME J. Dynam. Syst., Meas., Contr.*, vol. 118, no. 4, pp. 714–720, 1996.

[10] R. Vossoughi and M. Donath, "Dynamic feedback linearization for electro-hydraulically actuated control systems," *ASME J. Dynam. Syst., Meas., Contr.*, vol. 117, no. 4, pp. 468–477, 1995.

[11] L. D. Re and A. Isidori, "Performance enhancement of nonlinear drives by feedback linearization of linear-bilinear cascade models," *IEEE Trans. Contr. Syst. Technol.*, vol. 3, pp. 299–308, May 1995.

[12] B. Yao, G. T. C. Chiu, and J. T. Reedy, "Nonlinear adaptive robust control of one-dof electro-hydraulic servo systems," in *Proc. ASME IMECE'97*, vol. 4, Dallas, TX, 1997, pp. 191–197.

[13] B. Yao and M. Tomizuka, "Smooth robust adaptive sliding mode control of robot manipulators with guaranteed transient performance," in *Proc. American Control Conf.*, 1994, pp. 1176–1180.

[14] B. Yao and M. Tomizuka, "Adaptive robust control of SISO nonlinear systems in a semi-strict feedback form," *Automatica*, vol. 33, no. 5, pp. 893–900, 1997.

[15] B. Yao, "High performance adaptive robust control of nonlinear systems: A general framework and new schemes," in *Proc. IEEE Conf. Decision and Control*, 1997, pp. 2489–2494.

[16] B. Yao and M. Tomizuka, "Adaptive robust control of MIMO nonlinear systems," in *Proc. IEEE Conf. Decision and Control*, 1995, pp. 2346–2351.

[17] B. Yao, F. Bu, and G. T. C. Chiu, "Nonlinear adaptive robust control of electro-hydraulic servo systems with discontinuous projections," in *Proc. IEEE Conf. Decision and Control*, 1998, pp. 2265–2270.

[18] B. Yao, M. Al-Majed, and M. Tomizuka, "High performance robust motion control of machine tools: An adaptive robust control approach and comparative experiments," *IEEE/ASME Trans. Mechatron.*, vol. 2, pp. 63–76, June 1997.

[19] A. Alleyne, "Nonlinear force control of an electro-hydraulic actuator," in *Proc. Japan/USA Symp. Flexible Automation*, Boston, MA, 1996, pp. 193–200.

[20] M. Krstic, I. Kanellakopoulos, and P. V. Kokotovic, *Nonlinear and Adaptive Control Design*. New York: Wiley, 1995.

[21] S. Sastry and M. Bodson, *Adaptive Control: Stability, Convergence and Robustness*. Englewood Cliffs, NJ: Prentice-Hall, Inc., 1989.

[22] G. C. Goodwin and D. Q. Mayne, "A parameter estimation perspective of continuous time model reference adaptive control," *Automatica*, vol. 23, no. 1, pp. 57–70, 1989.

[23] H. K. Khalil, *Nonlinear Systems*, 2nd ed. Englewood Cliffs, NJ: Prentice-Hall, Inc., 1996.

[24] *Servo Tuner User Guide*, Parker Hannifin Company, Cleveland, OH, Nov. 1994.

[25] B. Yao and M. Tomizuka, "Smooth robust adaptive sliding mode control of robot manipulators with guaranteed transient performance," *ASME J. Dynam. Syst., Meas., Contr.*, vol. 118, no. 4, pp. 764–775, 1996.


**Bin Yao** (S'92–M'96) received the B.Eng. degree in applied mechanics from Beijing University of Aeronautics and Astronautics, Beijing, China, the M.Eng. degree in electrical engineering from Nanyang Technological University, Singapore, and the Ph.D. degree in mechanical engineering from the University of California, Berkeley, in 1987, 1992, and 1996, respectively.

Since 1996, he has been an Assistant Professor in the School of Mechanical Engineering, Purdue University, West Lafayette, IN. His research interests include design and control of intelligent high-performance coordinated control of electromechanical/electrohydraulic systems, optimal adaptive and robust control, nonlinear observer design and neural networks for virtual sensing, modeling, fault detection, diagnostics, and adaptive fault-tolerant control, and data fusion.

Dr. Yao was awarded a Faculty Early Career Development (CAREER) Award from the National Science Foundation (NSF) in 1998 for his work on the engineering synthesis of high-performance adaptive robust controllers for mechanical systems and manufacturing processes. He received the Caterpillar Engineering Young Faculty Development Award in 1997.

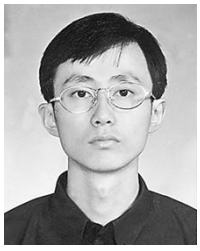

**Fanping Bu** received the B. Eng. and M.Eng. degrees in mechanical engineering from Tsinghua University, Beijing, China, in 1994 and 1997, respectively. He is currently working toward the Ph.D. degree at Purdue University, West Lafayette, IN.

His current research interests include adaptive control, robust control, robotics, and control of electrohydraulic systems.

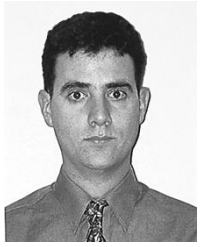

**John Reedy** was born in Los Alamos, NM, in 1973. He received the B.S.M.E. degree from the University of California, San Diego, in 1996. He is currently working toward the Master's degree at Purdue University, West Lafayette, IN, specializing in the design and control of high-performance electrohydraulic systems.

He is also currently with Caterpillar Inc., Peoria, IL, analyzing and designing electrohydraulic control systems for mobile equipment.

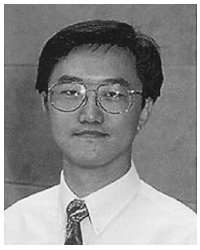

**George T.-C. Chiu** received the B.S.M.E. degree from National Taiwan University, Taipei, Taiwan, R.O.C., and the M.S. and Ph.D. degrees from the University of California, Berkeley, in 1985, 1990, and 1994, respectively.

From 1994 to 1996, he was an R&D Engineer with Hewlett-Packard Company, developing high-performance color inkjet printers and multifunction machines. Since 1996, he has been an Assistant Professor and a Feddersen Fellow in the School of Mechanical Engineering, Purdue University, West Lafayette, IN. His current research interests are design and control of imaging and printing systems, signal and image processing, adaptive and optimal control, integrated design and control of electromechanical systems, and mechatronics.